Available online at www.sciencedirect.com
ScienceDirect
Engineering Fracture Mechanics 75 (2008) 3806–3818
Engineering Fracture Mechanics
www.elsevier.com/locate/engfracmech

Determination of the kink point in the bilinear softening model for concrete

Kyoungsoo Park, Glaucio H. Paulino *, Jeffery R. Roesler

Department of Civil and Environmental Engineering, University of Illinois at Urbana-Champaign, 205 N., Mathews Avenue, Urbana, IL 61801-23552, USA

Received 15 October 2007; received in revised form 31 January 2008; accepted 5 February 2008
Available online 15 February 2008

Abstract

The characterization of the softening curve from experimental results is essential for predicting the fracture behavior of quasi-brittle materials like concrete. Among various shapes (e.g. linear, exponential) to describe the softening behavior of concrete, the bilinear softening relationship has been extensively used and is the model of choice in this work. Currently, there is no consensus about the location of the kink point in the bilinear softening curve. In this study, the location of the kink point is proposed to be the stress at the critical crack tip opening displacement. Experimentally, the fracture parameters required to describe the bilinear softening curve can be determined with the "two-parameter fracture model" and the total work of fracture method based on a single concrete fracture test. The proposed location of the kink point compares well with the range of kink point locations reported in the literature, and is *verified* by plotting stress profiles along the expected fracture line obtained from numerical simulations with the cohesive zone model. Finally, prediction of experimental load versus crack mouth opening displacement curves *validate* the proposed location of the kink point for different concrete mixtures and also for geometrically similar specimens with the same concrete mixture. The experiments were performed on three-point bending specimens with concrete mixtures containing virgin coarse aggregate, recycled concrete coarse aggregate (RCA), and a 50–50 blend of RCA and virgin coarse aggregate. The verification and validation studies support the hypothesis of the kink point occurring at the critical crack tip opening displacement.

Keywords: Concrete; Fracture; Bilinear softening; Kink point; Cohesive zone model; Two-parameter fracture model (TPFM)

1. Introduction

A characteristic behavior of concrete fracture is the relatively large fracture process zone, which can be represented by a softening model. A softening model can be determined either by concrete material fracture parameters or by an inverse analysis. Table 1 summarizes several published softening models based on concrete material fracture parameters. The concept of a cohesive crack was expanded to concrete by Hillerborg

* Corresponding author. Tel.: +1 217 333 3817; fax: +1 217 265 8041.
E-mail addresses: kpark16@uiuc.edu (K. Park), paulino@uiuc.edu (G.H. Paulino), jroesler@uiuc.edu (J.R. Roesler).

0013-7944/$ - see front matter © 2008 Elsevier Ltd. All rights reserved.
doi:10.1016/j.engfracmech.2008.02.002

Nomenclature

C_i	loading compliance
C_u	unloading compliance
$CTOD_c$	critical crack tip opening displacement
D	depth of beam specimens
E	elastic modulus of concrete
G_F	total fracture energy
G_f	initial fracture energy
K_{IC}	critical stress intensity factor
L	length of beam specimens
P	applied load on beam specimens
S	span of beam specimens
a_0	initial notch length of beam specimens
c_f	effective fracture process zone length
f'_t	concrete tensile strength
t	thickness of beam specimens
w	crack opening width
w_{cr}	critical crack opening width
w_f	final crack opening width
w_k	kink point of the crack opening width
w_1	horizontal intercept of the initial softening slope; and
ψ	stress ratio at the kink point

Table 1
Softening models for concrete

Hillerborg [1]	Linear softening curve (G_F, f'_t)
Petersson [2]	Bilinear softening curve (G_F,f'_t)
Gustafsson and Hillerborg [3]	Fixed kink point at ($0.8G/f'_t$, $f'_t/3$)
Wittmann et al. [4]	Bilinear softening curve (G_F, f'_t) Fixed stress kink point, $0.25f'_t$
CEB-90 model code [5]	Bilinear softening curve (G_F, f'_t, maximum aggregate size) Fixed stress kink point, $0.15f'_t$
Guinea et al. [6]	Bilinear softening curve (G_F, f'_t) Two additional empirical parameter to determine kink point
Bazant [24]	Bilinear softening curve (G_F, G_f, f'_t) Assume the stress ratio of the kink point (ψ).

et al. [1], who combined fracture mechanics, a linear softening curve, and the finite element method. The linear softening curve was defined by the tensile strength (f'_t) and the total fracture energy (G_F). Petersson [2] later proposed a bilinear softening curve whose kink point coordinates were fixed at ($0.8G_F/f'_t$, $f'_t/3$) though, ideally, an actual cohesive law should be a smooth function. This model was also adopted by Gustafsson and Hillerborg [3]. Wittmann et al. [4] defined a bilinear softening curve with a kink point stress of $0.25f'_t$ for their numerical analysis. The CEB-90 model code [5] recommended a bilinear softening curve for ordinary concrete fracture which could be described by the concrete's tensile strength, the total fracture energy, the maximum aggregate size, and a kink point stress of $0.15f'_t$. Guinea et al. [6] developed a general bilinear fit (or GBF) by means of a bilinear softening curve using tensile strength, total fracture energy, and two empirical parameters representing the shape of the softening curve. The aforementioned softening models have mainly been defined by two measured fracture parameters (f'_t and G_F).

Alternatively, a softening curve can be also inferred from inverse analysis [7]. Such inverse analysis is generally based on optimization procedures which minimize the difference between simulation results and exper-

imental results. Kitsutaka [8] obtained a polylinear softening model using an experimental load–displacement curve. Planas et al. [9] determined the initial portion of a softening curve based on measured peak loads. Elices et al. [10] refined the GBF in conjunction with an inverse analysis. Abdalla and Karihaloo [11] utilized an inverse analysis to construct a bilinear softening based on a non-linear hinge model with the true specific fracture energy [12,13]. Recently, Sousa and Gettu [14], and Slowik et al. [15] proposed an optimization procedure to improve uniqueness of the inverse analysis results. Although the inverse analysis would provide the best fit to experimental results because optimization algorithms are utilized, this paper focuses on the former approach which determines a softening model in conjunction with physical fracture parameters.

The essential fracture parameter in a softening model is the total fracture energy which corresponds to the area under the softening curve. The total fracture energy evaluated by the work-of-fracture method [16] depends on specimen sizes [17–21], and Hillerborg reported that the calculated strength of structure is not as sensitive to the value of G_F [22]. Abdalla and Karihaloo [12,13] introduced the size-independent specific fracture energy through consideration of boundary effect and local fracture energy distribution. In order to describe concrete fracture behaviour in conjunction with size independent fracture parameters, Jenq and Shah [23] proposed the two parameter fracture model (TPFM). The model is based on the concept of an equivalent elastic crack and calculates the following two size independent fracture parameters: critical stress intensity factor (K_{IC}) and the elastic critical crack tip opening displacement ($CTOD_c$). These two parameters are derived from the experimental loading-unloading procedure as illustrated in Fig. 1, which separates the elastic response ($CMOD_{ec}$) from the inelastic response ($CMOD_{pc}$), and ultimately provides the loading compliance (C_i) and the unloading compliance (C_u) of a concrete specimen.

Recently, Bazant [24] further defined the bilinear softening curve with the measured initial fracture energy (G_f). Since the initial fracture energy controls the maximum loads of structures and thus the size effect [24,25], it is defined as the area under the initial ascending and descending slopes of the softening model [26] as shown in Fig. 2. The initial fracture energy, therefore, defines the horizontal axis intercept (w_1) of the initial softening slope (see Fig. 2), expressed as

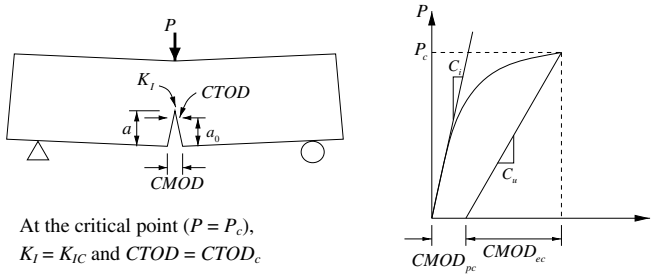

Fig. 1. Schematic illustration of the two parameter fracture model [23].

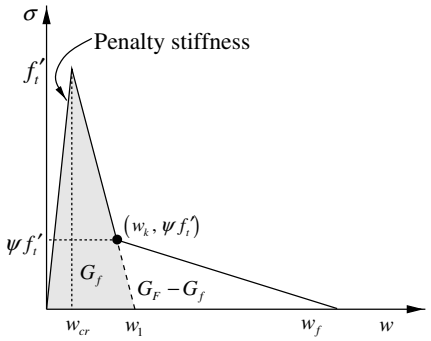

Fig. 2. Bilinear softening curve for concrete.

$$w_1 = \frac{2G_f}{f'_t}. \tag{1}$$

In addition, the final crack opening width (w_f), in Fig. 2, is readily calculated as

$$w_f = \frac{2}{\psi f'_t}[G_F - (1-\psi)G_f], \tag{2}$$

which is obtained by assuming the stress ratio at the kink point (ψ) and by equating the total fracture energy (G_F) with the area under the bilinear softening curve. Bazant [24] also estimated the kink point at the stress change to be in the range between $0.15f'_t$ and $0.33f'_t$.

Though the bilinear softening curve is routinely employed for the cohesive law of concrete fracture behavior [5,10,27], there hasn't been a consensus about the location of the kink point for different concrete mixtures [28]. The kink point stress ratios proposed by other authors (e.g., 0.33, 0.25, and 0.15) are not directly derived from measured fracture properties, but are generally selected to give a reasonable reproduction of the global specimen fracture behavior (P-CMOD). In this paper, a method to determine the kink point for a bilinear softening model is proposed on the basis of experimental fracture parameters namely $CTOD_c$, G_f and f'_t. To validate the experimentally-based kink point location, a bilinear intrinsic cohesive zone model (Fig. 2) is used to predict load versus crack mouth opening displacement (CMOD) curves not only for different concrete mixtures but also for geometrically similar notched concrete beam specimens. The cohesive zone model is implemented using the finite element method.

2. Hypothesis of the kink point

The first and the second descending slopes in a bilinear softening curve are clearly defined by the concrete's initial and the total fracture energy. As indicated above, the stress ratio at kink point (ψ) is usually assumed to be between 0.15 and 0.33 without actual agreement on the precise location. Three parameters (f'_t, G_f and G_F) are currently used for the determination of the x-intercepts (w_1 and w_f) in a bilinear softening curve as shown in expressions (1) and (2). Based on the TPFM, a fourth fracture parameter, $CTOD_c$, is calculated from the experimental testing but is not utilized in the modeling. The stress ratio at the kink point can be estimated on the basis of this fracture parameter.

Since the softening curve is a function of the crack opening width (w), the $CTOD_c$ can be utilized for the determination of the stress ratio at the kink point. The $CTOD_c$ magnitude is between the critical crack opening width (w_{cr}) and the final crack opening width (w_f) in the bilinear softening model ($w_{cr} < CTOD_c < w_f$). Based on the TPFM [29], $CTOD_c$ is calculated from the peak load of the specimen and therefore its position corresponds to the initial slope of the bilinear softening curve. The kink point of the crack opening width (w_k) is hypothesized as (see Fig. 2)

$$w_k = CTOD_c. \tag{3}$$

This is the key expression proposed in this paper. For specimens tested in this research program [30,31], the $CTOD_c$ values lie within the crack opening width range of the initial slope of the bilinear softening curve. Eq. (3) results in the stress ratio of the kink point, i.e.

$$\psi = \frac{w_1 - w_k}{w_1 - w_{cr}}. \tag{4}$$

Since $w_{cr} \ll w_1$, Eqs. (1) and (4) can be approximated as

$$\psi = 1 - \frac{CTOD_c f'_t}{2G_f}, \tag{5}$$

which enables determination of the whole bilinear softening curve based on four experimental fracture parameters (f'_t, G_f, G_F and $CTOD_c$) obtained from a single fracture test and a tensile strength test. The tensile strength can be indirectly inferred from the splitting test by considering the influence of specimen geometry (e.g. cylindrical and cubical specimens) and the width of the load-bearing strip [32,33]. The two fracture

parameters (G_f and $CTOD_c$) can be calculated by either the TPFM or the size effect method [34,35] as the two methods are equivalent [36].

3. Validation

Locations of the kink point calculated by Eq. (5) are examined by using experimental fracture parameters available in the literature. Selected data sets of experimental fracture parameters, based on the TPFM or size effect method [34,35], and concrete tensile strength, were used for the calculation of the kink point (ψ) as summarized in Table 2. It illustrates experimental concrete fracture parameters provided by Roesler et al. [30,31], Chang and Shieh [37], Jenq and Shah [23,38], and Karihaloo and Nallathambi [39,40]. The marked cells (*) in the initial fracture energy column are calculated by the following expression $G_f = K_{IC}^2/E$ where E is the elastic modulus for plane stress condition. The relationship between the initial fracture energy (G_f) and the critical stress intensity factor (K_{IC}) is confirmed by Planas and Elices [41]. In addition, the marked cells (*) in the $CTOD_c$ and the effective fracture process zone length (c_f) columns are determined from the following expression [42]

$$c_f = \frac{\pi}{32}\left(\frac{CTOD_c E}{K_{IC}}\right)^2 \tag{6}$$

Moreover, w_1 and ψ in Table 2 are calculated by expressions (1) and (5), respectively. One kink point stress ratio from Karihaloo and Nallathambi [39,40] was not available (N/A) since $CTOD_c$ was greater than w_1. As seen in Table 2, the entire range of the calculated kink point stress ratios is between 0.14 and 0.42, which is comparable to the range proposed by Bazant (0.15–0.33).

4. Verification

In order to verify the kink point location assumption, numerical simulations of the three-point beam-bending (TPB) test were implemented by using the cohesive zone model in a non-linear finite element framework. Similar simulations can also be accomplished with the fictitious crack model (FCM) [7,43]. The TPB test shown in Fig. 3 were tested by using geometrically similar beams with constant thickness ($t = 80$ mm), notch to depth ratio (a_0/D) of 1/3, and span to depth ratio (S/D) of 4 for each beam size. The laboratory experiments conducted were the second data set [31] in Table 2, which provides the four fracture parameters (f_t', G_f, G_F and $CTOD_c$) required for the determination of the bilinear softening material separation model of Fig. 2. The average concrete tensile strength ($f_t' = 4.15$ MPa) was attained by the split tensile test for this normal strength concrete mixture with a maximum aggregate size of 19 mm. The initial fracture energy of the concrete was

Table 2
Fracture parameters of concrete and calculated kink point stress ratio (ψ)

Reference	f_t' (MPa)	E (GPa)	K_{IC} (MPa m$^{1/2}$)	$CTOD_c$ (mm)	G_f (N/m)	c_f (mm)	w_1 (mm)	Ψ
Roesler et al. [30]	2.61	26	0.94	0.0158	34*	18.8*	0.026	0.393
	2.45	28	0.91	0.0159	29.6*	23.5*	0.0241	0.341
	2.84	24.7	0.85	0.0161	29.3*	21.5*	0.0206	0.218
Roesler et al. [31]	4.15	32	1.13	0.018	56.6	25.5	0.0273	0.34
Chang and Shieh [37]	2.92	22.3	0.91	0.0208*	37.1	25.4	0.0254	0.184
	3.16	19.7	0.82	0.0136*	34.1	10.4	0.0216	0.373
Jenq and Shah [23,28]	2.57	33.6	1.09	0.016	35.4	23.9*	0.0275	0.419
	3.14	25.4	0.732	0.0092	21.1	10*	0.0134	0.315
	4.29	32.5	0.958	0.0097	28.2	10.6*	0.0132	0.263
	4.41	37.3	1.06	0.01	30.1	12.2*	0.0136	0.267
Karihaloo and Nallathambi [39,30]	2.58	24.6	0.992	0.0332	40*	66.6*	0.031	N/A
	3.11	33.8	1.27	0.0263	47.3*	48.5*	0.0305	0.136
	3.5	34.7	1.38	0.0261	54.6*	42.5*	0.0312	0.163
	4.09	37.2	1.5	0.0242	60.7*	35.3*	0.0297	0.184
	4.41	40.3	1.88	0.0262	87.8*	30.9*	0.0398	0.342

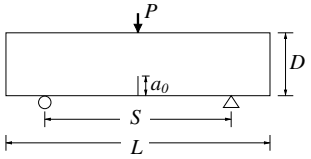

D (mm)	S (mm)	L (mm)	a_0 (mm)	t (mm)	G_f (N/m)	G_F (N/m)
63	250	350	21	80	56.6	119
150	600	700	50	80	56.6	164
250	1000	1100	83	80	56.6	167

Fig. 3. Geometry and fracture properties of test specimens.

56.6 N/m, obtained by the TPFM. The average G_F for the specimens with 250, 150, and 63 mm depth, was 167, 164, and 119 N/m, respectively, as shown in Fig. 3. The stress ratio at the kink point (ψ) was calculated by equating the kink point of the crack opening width (w_k) with the $CTOD_c$. The stress ratio of 0.34 was determined for this concrete mixture, and the resultant stress at the kink point ($\psi f_t'$) was 1.41 MPa, based on the definition of the kink point given in (5).

The initial numerical simulation had a beam depth (D) of 63 mm. The resultant cohesive zone model was implemented into the commercial finite element software, ABAQUS as a user-defined element (UEL) subroutine. In the UEL, the contributions of cohesive elements to the tangent stiffness matrix and the load vector are evaluated on the basis of the intrinsic-based traction-separation constitutive relationship. Fig. 4 illustrates the finite element mesh for the simulation. Volumetric elements were used for the uncracked regions of the concrete and cohesive surface elements were employed in the region of the expected fracture, as shown in Fig. 4b. The size of the cohesive element was selected to be 1 mm, which is small enough to capture the local fracture process in this problem [31]. Displacement boundary conditions are applied to the loading region. Further implementation details can be found elsewhere and the reader is referred to publications [31,44–46]. Fig. 5 shows the predicted numerical simulation of the load versus CMOD for the TPB specimen.

Through numerical simulations, the stress profile along the crack propagation direction was examined at three different points: the pre-peak load (point A), the peak load (point B) and the post-peak load (point C) as described in the load-CMOD curves in Fig. 5. The stress profiles were evaluated either by averaging the stress at the node (solid line) or by substituting the crack opening width into the bilinear constitutive model (dashed line), as shown in Fig. 6. At the pre-peak load (point A), the stress at the tip of the initial notch (a_0) is higher than the stress at the kink point (1.41 MPa) as shown in Fig. 6a. When the load reaches the peak point B, the stress at the tip of the initial notch (a_0) nearly corresponds to the stress at the kink point (Fig. 6b). After the peak load, the stress profile along the crack propagation direction (Fig. 6c) demonstrates a large change of slope around the stress kink point, which resembles the bilinear softening curve. In summary, when the stress

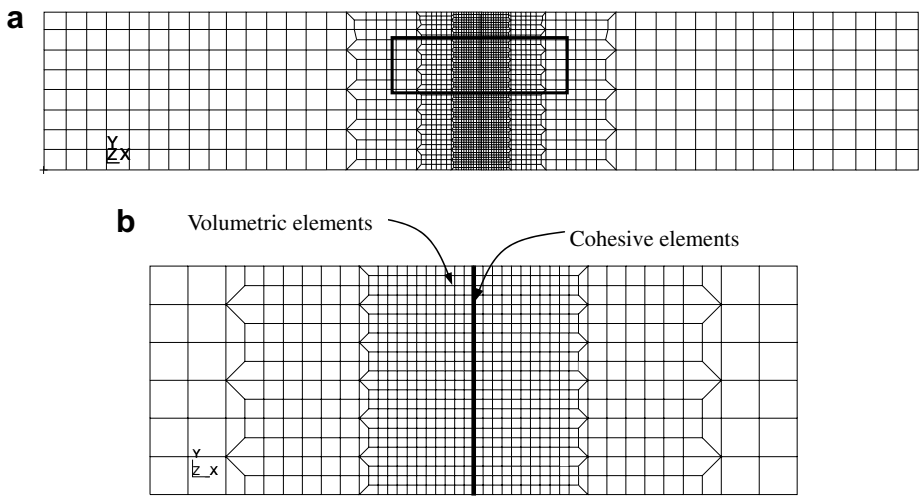

Fig. 4. (a) Finite element mesh for specimen size $D = 63$ mm, and (b) zoom of mesh along the cohesive element region.

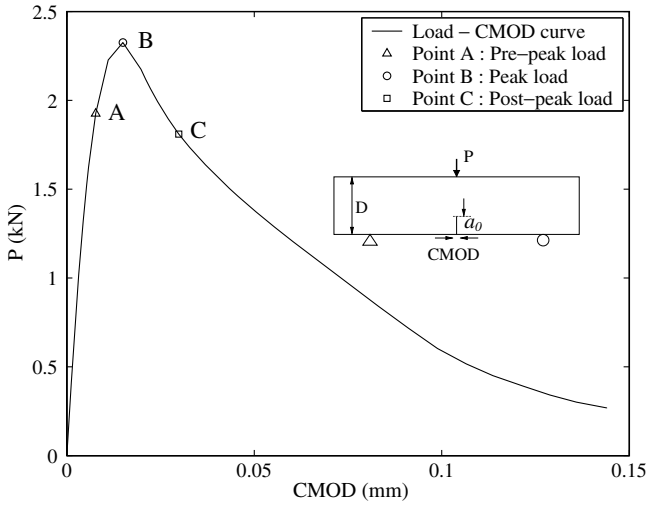

Fig. 5. Numerical result of a load-CMOD curve for a small-size beam ($D = 63$ mm).

at the tip of the initial notch approximately reaches the stress at the kink point ($\psi f_t'$), the numerical simulations produced the maximum load capacity (point B) for the TPB specimen. A similar stress profile behavior was captured along the crack propagation direction for a larger beam size ($D = 250$ mm) based on the same numerical simulations.

5. Numerical predictions of concrete fracture behavior

The proposed bilinear softening model is utilized to predict fracture behavior not only of different concrete mixtures but also for geometrically similar specimens of the same concrete mixture. These predictions will validate the proposed kink point stress ratio definition in the bilinear softening model.

5.1. Different concrete mixtures with the same geometry

To validate the proposed softening model for different concrete mixtures, the three-point beam bending (TPB) tests reported by Roesler et al. [30] were utilized. The concrete beams were cast with two different coarse aggregate types, i.e., virgin aggregates, recycled coarse aggregates (RCA) and a 50% blend of the RCA and virgin coarse aggregates [30]. The geometry of the tests is provided in Fig. 3, and the beam depth was 150 mm for all the tests. The average total fracture energy of concrete with virgin coarse aggregate had the highest value of 85.9 N/m. The total fracture energy of the RCA and of the 50–50 blend mixtures were 55.5 and 84.8 N/m, respectively. Other evaluated fracture parameters for three different aggregate types (virgin aggregate, RCA, and 50–50 blend) are provided in the first three data sets in Table 2, respectively. Based on the measured fracture parameters, the proposed bilinear softening model predicts load versus CMOD curves for the different concrete mixtures. Fig. 7a–c demonstrates the agreements of numerical predictions and experimental results for the concrete mixtures containing virgin and recycled concrete coarse aggregate. Both the computational and experimental results show that the concrete mixture with virgin coarse aggregates is able to dissipate more energy than the mixture with RCA.

5.2. Geometrically similar specimens with the same concrete Mixture

In addition to the investigation of the different concrete mixtures, the proposed bilinear softening model was applied to predict fracture behavior of geometrically similar specimens. The experiments reported by Roesler et al. [31] were utilized in this study. The beam depths (D) were 63, 150, and 250 mm with a thickness

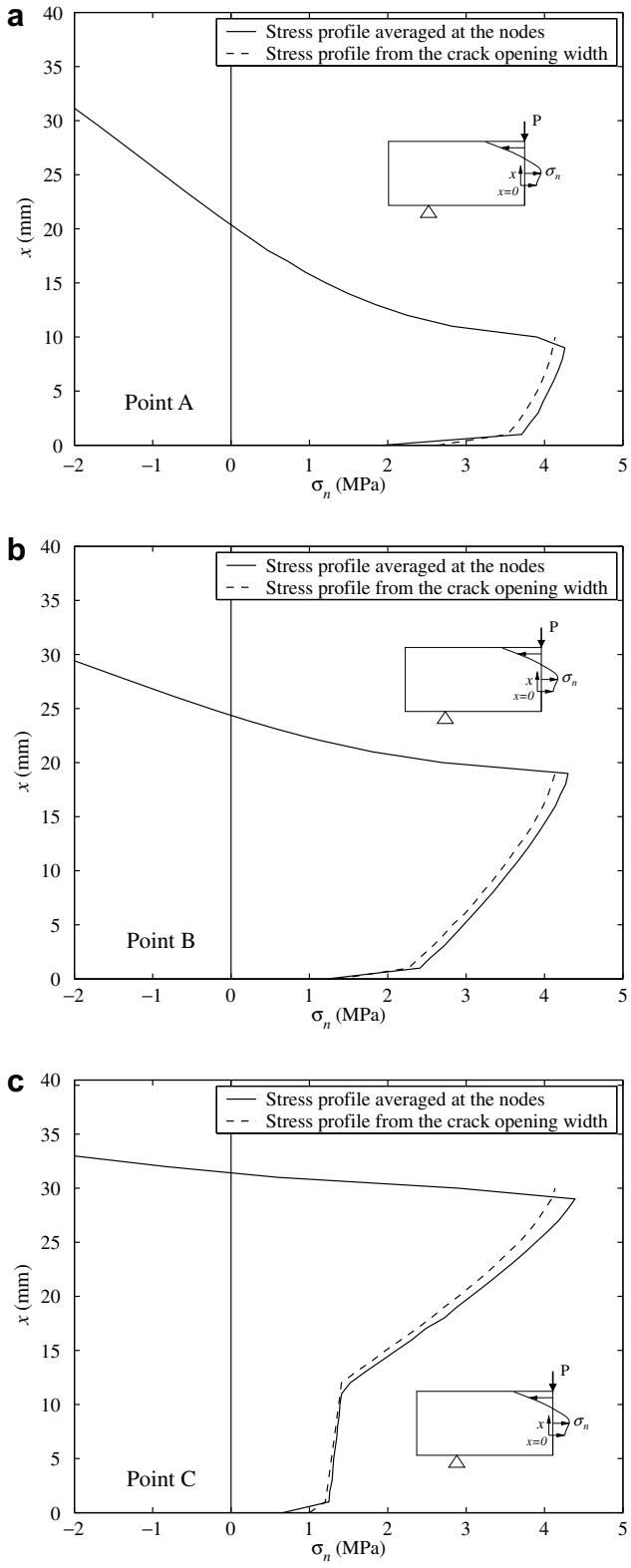

Fig. 6. (a) Surface normal stress (σ_n) profile along the crack propagation direction at point A, (b) at point B and (c) at point C in the load-CMOD curve.

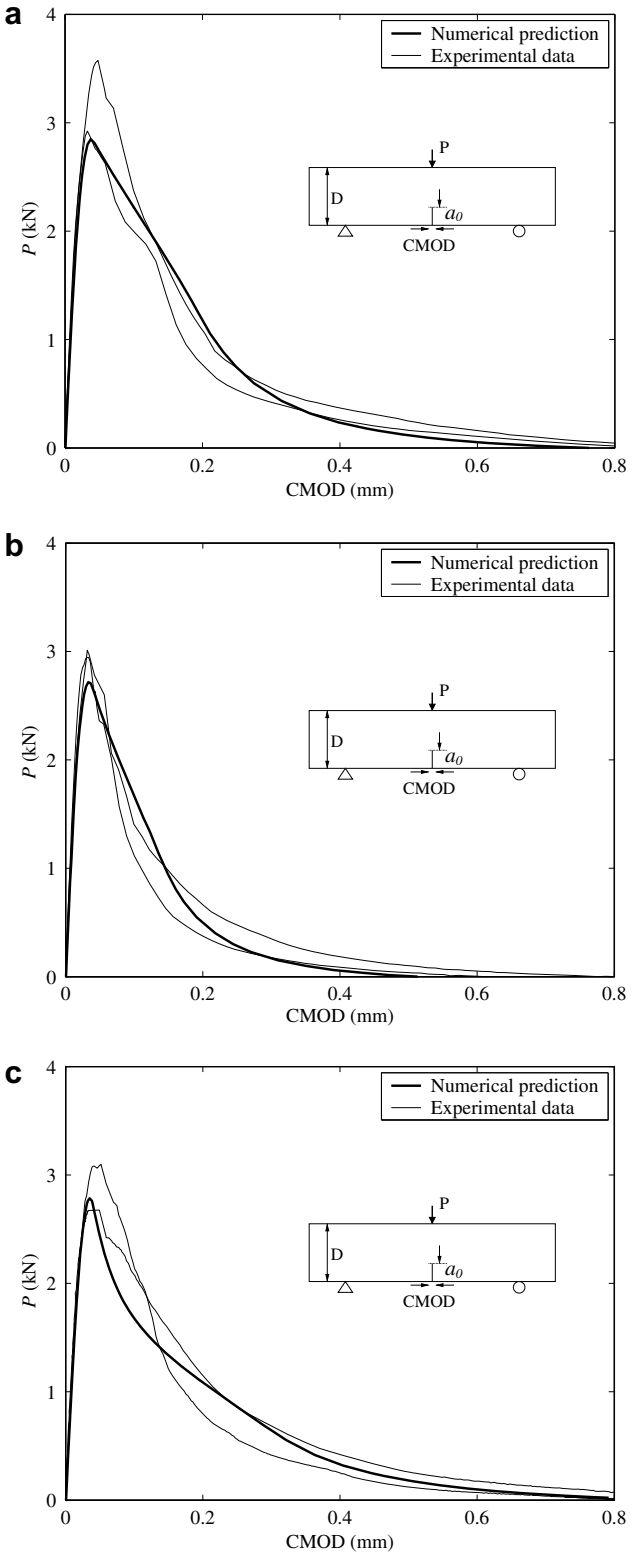

Fig. 7. Comparison between experimental and numerical results for different concrete mixtures: (a) Virgin coarse aggregate concrete; (b) recycled coarse aggregate concrete; and (c) 50–50 blend of virgin and RCA concrete.

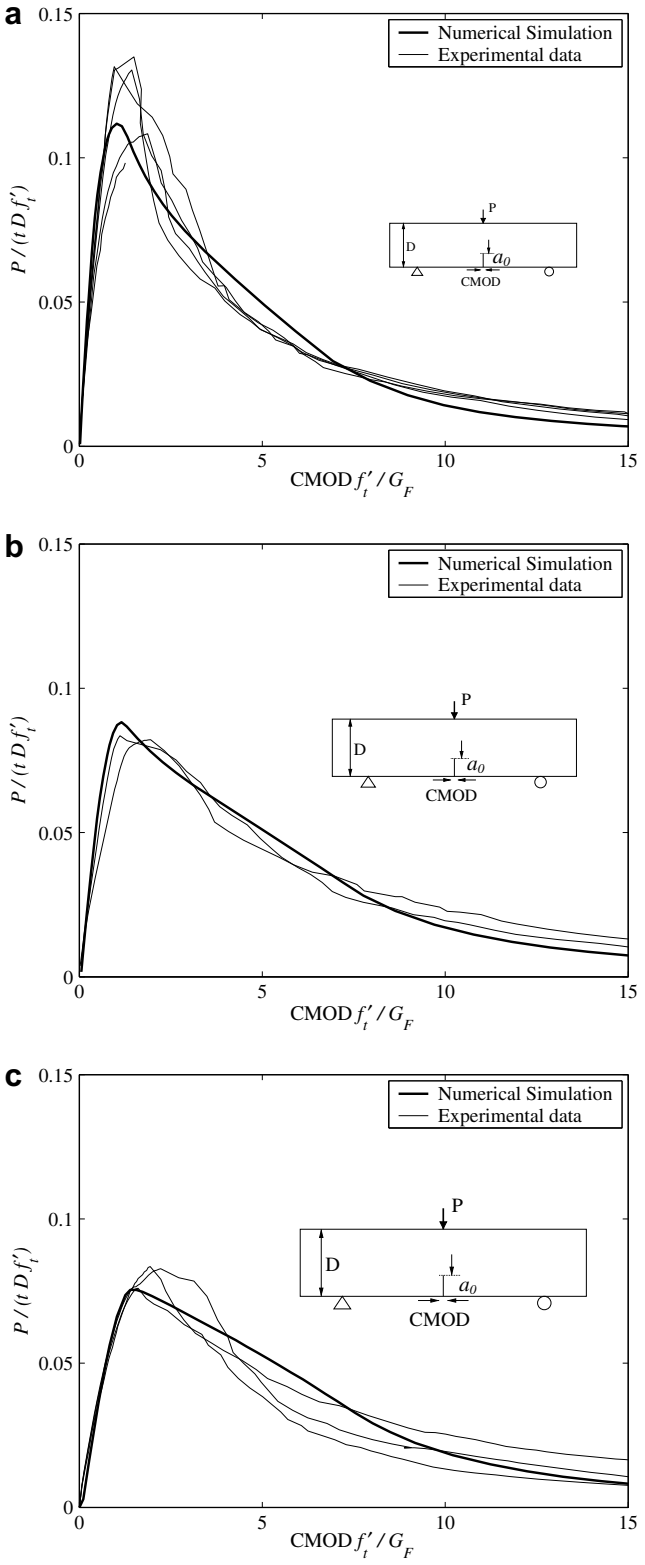

Fig. 8. Numerical predictions of normalized load-CMOD curves compared with experimental data: (a) specimen size, $D = 63$ mm, (b) specimen size, $D = 150$ mm, (c) specimen size, $D = 250$ mm.

of 80 mm. The total fracture energy increased with respect to increasing specimen size, as shown in Fig. 3. The numerical simulation employing the bilinear softening model predicted the load (P) versus CMOD curves for each specimen size with the second data set in Table 2 [31]. Fig. 8a–c illustrates the correspondence between the numerical predictions and the experimental results for each specimen size with respect to the normalized P-CMOD ($P/(tDf'_t)$ – CMODf'_t/G_F) curve. For comparison purposes, all the plots are provided on the same scales for the horizontal and vertical axis. If strength of the beam specimen is assumed to be proportional to P/Dt [28], both experimental and numerical results demonstrate the decrease of nominal specimen strength with respect to the increase in the specimen size (D), which is a manifestation of the size effect.

For the bilinear material traction-separation model of Fig. 2, the initial fracture energy (G_f) and the tensile strength (f'_t) are essential parameters to determine the maximum strength of the specimens, while the stress ratio at the kink point (ψ) and the total fracture energy (G_F) influence the post-peak behavior [46], as shown in Fig. 9, for this specimen geometry and boundary conditions. The sensitivity of ψ to the post-peak load behavior was examined through the different stress ratios of the kink point (0.15 and 0.34), as shown in Fig. 10, for the same f'_t, G_f, and G_F. Fig. 10 illustrates that the proposed location of the kink point provides reasonable post-peak load behavior with the experimental data [31] in Table 2. Wittman et al. [4] showed the kink point stress affected the specimen's peak load when the initial slope was allowed to change, implying a change in the G_f. In the simulation presented in Fig. 10, the initial fracture energy (G_f) was fixed. Therefore, the magnitude of the kink point stress did not affect the calculated peak load as the kink point stress ratio increased from 0.15 to 0.34.

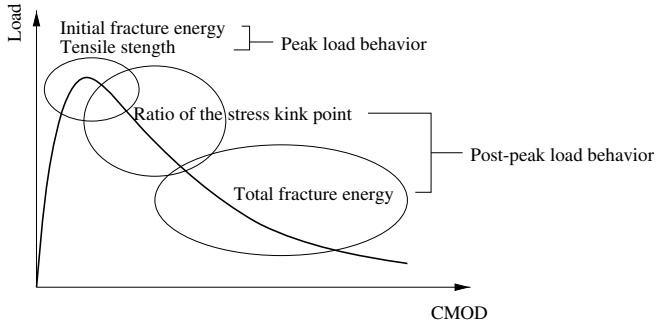

Fig. 9. Sensitivity of the numerical prediction of a load-CMOD curve for the four fracture parameters (f'_t, G_f, G_F and ψ).

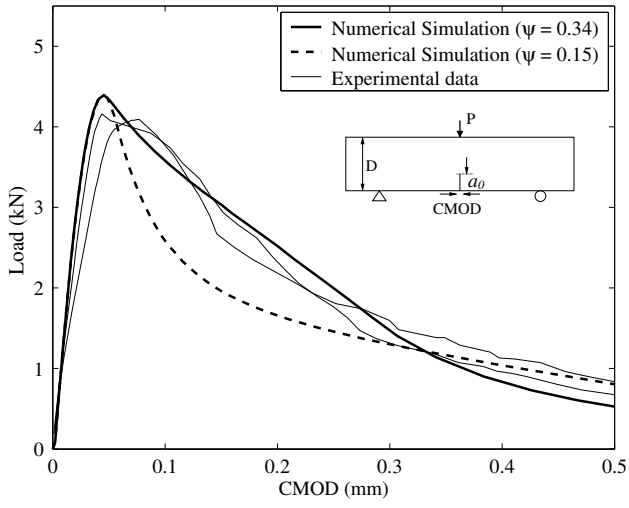

Fig. 10. Sensitivity of the stress ratio at the kink point to predicted load-CMOD curves ($D = 150$ mm) for experimental data in Ref. [31].

6. Conclusion

The location of the kink point is hypothesized on the basis of experimental fracture parameters. The kink point of the crack opening width (w_k) is proposed to be the same as the critical crack tip opening displacement ($CTOD_c$). This practical assumption leads to the direct determination of the whole bilinear softening curve, based on the four experimental fracture parameters (f'_t, G_f, G_F and $CTOD_c$) which can be obtained from a standard concrete fracture test. Therefore, there is no need to arbitrarily assume the kink point stress ratio, or to calibrate the softening model to fit the numerical results with experimental concrete fracture results.

The proposed location of the kink point compares with the range of the kink point locations presented in the literature, and is verified by plotting stress profile along the cohesive zone in the numerical simulations. In order to provide some validation for the proposed location of the kink point, experimental load-CMOD curves were predicted using the cohesive zone model not only for different concrete mixtures but also for geometrically similar specimens. Although other softening models may provide better fit to a set of experimental results (e.g., inverse analysis), the proposed linkage between the kink point in the bilinear softening curve and the $CTOD_c$ is now systematically defined rather than being arbitrarily pre-defined or empirically calibrated.

Acknowledgements

This paper was prepared from a study conducted in the "Center of Excellence for Airport Technology (CEAT)," funded by the Federal Aviation Administration (FAA) under Research Grant No. 95-C-001 and the University of Illinois. The contents of this paper reflect the views of the authors, who are responsible for the facts and accuracy of the data presented within. The contents do not necessarily reflect the official views and policies of the sponsors. This paper does not constitute a standard, specification, or regulation.

References

[1] Hillerborg A, Modeer M, Petersson PE. Analysis of crack formation and crack growth in concrete by means of fracture mechanics and finite elements. Cement Concrete Res 1976;6(6):773–82.
[2] Petersson PE. Crack growth and development of fracture zone in plain concrete and similar materials. Report No. TVBM-1006, Division of building materials, Lund Institute of Technology, Lund, Sweden; 1981.
[3] Gustafsson A, Hillerborg PJ. Improvements in concrete design achieved through application of fracture mechanics. In: Shah SP, editor. Application of fracture mechanics to cementitious composites. The Netherlands: Dordrecht; 1985. p. 639–80.
[4] Wittmann FH, Rokugo K, Bruhwiler E, Mihashi H, Simopnin P. Fracture energy and strain softening of concrete as determined by compact tension specimens. Mater Struct 1988;21(1):21–32.
[5] CEB-90. Final draft CEB-FIP mode code 1990. Bulletin information 203, Committee Euro-International du Beton, 1991.
[6] Guinea GV, Planas J, Elices M. A general bilinear fit for the softening curve of concrete. Mater Struct 1994;27(2):99–105.
[7] Roelfestra PE, Wittmann FH. Numerical method to link strain softening with failure of concrete. In: Wittmann FH, editor. Fracture toughness and fracture energy of concrete. Amsterdam: Elsevier Science Publishers; 1986. p. 163–75.
[8] Kitsutaka Y. Fracture parameters by polylinear tension-softening analysis. J Engng Mech – ASCE 1997;123(5):444–50.
[9] Planas J, Guinea GV, Elices M. Size effect and inverse analysis in concrete fracture. Int J Fract 1999;95:367–78.
[10] Elices M, Guinea GV, Gomez J, Planas J. The cohesive zone model: advantages, limitations and challenges. Engng Fract Mech 2002;69(2):137–63.
[11] Abdalla HM, Karihaloo BL. A method for constructing the bilinear tension softening diagram of concrete corresponding to its true fracture energy. Mag Concrete Res 2004;56(10):597–604.
[12] Abdalla HM, Karihaloo BL. Determination of size-independent specific fracture energy of concrete from three-point bend and wedge splitting tests. Mag Concrete Res 2003;55(2):133–41.
[13] Karihaloo BL, Abdalla HM, Imjai T. A simple method for determining the true specific fracture energy of concrete. Mag Concrete Res 2003;55(5):181–471.
[14] Sousa JLAO, Gettu R. Determining the tensile stress-crack opening curve of concrete by inverse analysis. J Engng Mech – ASCE 2006;132(2):141–8.
[15] Slowik V, Villmann B, Bretschneider N, Villmann T. Computational aspects of inverse analyses for determining softening curves of concrete. Comput Method Appl Mech Engng 2006;195(52):7223–36.
[16] Hillerborg A. The theoretical basis of a method to determine the fracture energy G_F of concrete. Mater Struct 1985;16(4):291–6.
[17] Hillerborg A. Concrete fracture energy tests performed by 9 laboratories according to a draft RILEM recommendation. Report to RILEM TC 50-FMC, Division of building materials, Lund Institute of Technology, Sweden; 1983.
[18] Hillerborg A. Additional concrete fracture energy tests performed by 6 laboratories according to a draft RILEM recommendation, Report to RILEM TC 50-FMC, Division of building materials, Lund Institute of Technology, Sweden; 1984.

[19] Mindess S. The effect of specimen size on the fracture energy of concrete. Cement Concrete Res 1984;14(3):431–6.
[20] Nallathambi P, Karihaloo BL, Heaton BS. Various size effects in fracture of concrete. Cement Concrete Res 1985;15(1):117–26.
[21] Bazant ZP, Kazemi MT. Size dependence of concrete fracture energy determined by RILEM work-of-fracture method. Int J Fract 1991;51(2):121–38.
[22] Hillerborg A. Influence of beam size on concrete fracture energy determined according to a draft RILEM recommendation, Report TVBM-3021, Division of building materials, Lund Institute of Technology, Lund, Sweden; 1985.
[23] Jenq YS, Shah SP. Two parameter fracture model for concrete. J Engng Mech – ASCE. 1985;111(10):1227–41.
[24] Bazant ZP. Concrete fracture models: testing and practice. Engng Fract Mech 2002;29(2):165–205.
[25] Planas J, Elices M, Guinea GV. Measurement of the fracture energy using three-point bend tests: Part 2 – Influence of bulk energy dissipation. Mater Struct 1992;25(5):305–12.
[26] Bazant ZP, Yu Q, Zi G. Choice of standard fracture test for concrete and its statistical evaluation. Int J Fract 2002;118(4):303–37.
[27] Elices E, Planas J. Fracture mechanics parameters of concrete: an overview. Adv Cement Based Mater 1996;4:116–27.
[28] Bazant ZP, Planas J. Fracture and size effect in concrete and other quasibrittle materials. Boca Raton: CRC Press; 1998.
[29] Shah SP, Swartz SE, Ouyang C. Fract Mech Concrete. New York: John Wiley & Sons; 1995.
[30] Roesler J. Personal communication; 2007.
[31] Roesler J, Paulino GH, Park K, Gaedicke C. Concrete fracture prediction using bilinear softening. Cement Concrete Compos 2007;29(4):300–12.
[32] Rocco C, Guinea GV, Planas J, Elices M. Size effect and boundary conditions in the Brazilian test: experimental verification. Mater Struct 1999;32(3):210–7.
[33] Rocco C, Guinea GV, Planas J, Elices M. Review of the splitting-test standards from a fracture mechanics point of view. Cement Concrete Res 2001;31(1):73–82.
[34] Bazant ZP, Kazemi MT. Determination of fracture energy, process zone length and brittleness number from size effect, with application to rock and concrete. Int J Fract 1990;44(2):111–31.
[35] Bazant ZP. Size effect. Int J Solids Struct 2000;37(1–2):69–80.
[36] Ouyang C, Tianxi T, Shah SP. Relationship between fracture parameters from two parameter fracture model and from size effect model. Mater Struct 1996;29(2):79–86.
[37] Chang T-P, Shieh M-M. Fracture properties of lightweight concrete. Cement Concrete Res 1996;26(2):181–8.
[38] Jenq YS, Shah SP. A fracture toughness criterion for concrete. Engng Fract Mech 1985;21(5):1055–69.
[39] Karihaloo BL, Nallathambi P. Fracture toughness of plain concrete from three-point bend specimens. Mater Struct 1989;22(3):185–93.
[40] Karihaloo BL, Nallathambi P. Notched beam test: mode I fracture toughness. In: Shah SP, Carpinteri A, editors. Fracture mechanics test methods for concrete. London: Chapman & Hall; 1991. p. 1–86.
[41] Planas J, Elices M. Fracture criteria for concrete: mathematical approximations and experimental validation. Engng Fract Mech 1990;35(1–3):87–94.
[42] Bazant ZP, Becq-Giraudon E. Statistical prediction of fracture parameters of concrete and implications for choice of testing standard. Cement Concrete Res 2002;32(4):529–56.
[43] Mulule SV, Dempsey JP. Stress-separation curves for saline ice using fictitious crack model. J Engng Mech – ASCE 1997;123(8):870–7.
[44] Song SH, Paulino GH, Buttlar WG. Simulation of crack propagation in asphalt concrete using a cohesive zone model. J Engng Mech – ASCE 2006;132(11):1215–23.
[45] Song SH, Paulino GH, Buttlar WG. A bilinear cohesive zone model tailored for fracture of asphalt concrete considering viscoelastic bulk material. Engng Fract Mech 2006;73(18):2829–48.
[46] Park K. Concrete fracture mechanics and size effect using a specialized cohesive zone model. Master thesis, University of Illinois at Urbana-Champaign, 2005.